Intramolecular Electronic and Hydrogen-Bonding Interactions in *N,N′*-Dimethyl-2,3-di-*O*-methyl-L-tartaramide

Carlos Alemán* and Sergio E. Galembeck†

Departament d'Enginyeria Química, E.T. S. d'Enginyers Industrials de Barcelona, Universitat Politècnica de Catalunya, Diagonal 647, Barcelona E-08028, Spain

Received November 6, 1996[⊗]

The changes in energy of the *N,N′*-dimethyl-2,3-di-*O*-methyl-L-tartaramide, model compound of polytartaramides based on 2,3-di-*O*-methyl-L-tartaric acid and 1,*n*-alkanediamine, have been analyzed by ab initio quantum mechanical calculations. The influences of the *gauche* oxygen effect have been investigated in the gas phase as well as in aqueous, chloroform, and carbon tetrachloride solutions. The results indicate that polarizable environments enhance the *gauche* oxygen effect, but the amount of stabilization depends on the electronic characteristics of the solvent.

Introduction

It is well-known that the C−C bond in the O−C−C−O sequence of ethers and alcohols often prefers the *gauche* conformation over the *trans* one.[1−4] Thus, the so-called *gauche* oxygen effect has been extensively investigated during the past years in simple model compounds such as nucleosides and nucleotides[4−7] as well as small diethers.[8−11] The influence of the environment on the *gauche* oxygen effect has been recently investigated by both experimental[12−15] and theoretical[8,9] methodologies. Results indicate that polarizable media increase the stability of the *gauche* conformation with respect to the *trans* one. For instance, the analysis of vicinal $^1H-^1H$ coupling constants of 1,2-dimethoxyethane (CH_3OCH_2-CH_2OCH_3), abbreviated 1,2-DME, reveals that the stability of the *gauche* conformation with respect to the *trans* one is −0.4 and −1.2 kcal/mol in vapor phase and aqueous solution, respectively.

Recently, Muñoz-Guerra and co-workers have reported on the synthesis, structure, and properties of polytartaramides.[16−20] Among the different types of polytartaramides that have been investigated by the authors, those based on 2,3-di-*O*-methyl-L-tartaric acid and 1,*n*-alkanediamine, named PnDMLTs, have been the subject of preferential attention.[17−20]

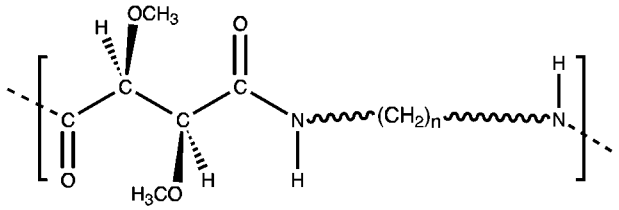

These are stereoregular polyamides that display high crystallinity and show large optical activity in solution. They exhibit a pronounced affinity for water and hydrolyze faster than conventional polyamides. X-ray diffraction studies reveal that the molecular structure of PnDMLTs are defined by the tartaric unit.[19,20] Thus, it was found that the preferred conformation for such polymers entailed the tartaric acid moiety in a *gauche* arrangement with the amide groups rotated out of the plane containing the *all-trans* polymethylene segment. Note that the tartaric acid moiety contains four oxygen atoms, which are able to define three O−C−C−O sequences. Furthermore, it contains two polar hydrogen atoms able to form intramolecular hydrogen bonds with the oxygen atoms of both the carbonyl and ether groups. In order to clarify the *gauche* oxygen effect in the tartaric acid unit of PnMDLT, it is useful to carry out a conformational analysis of its model compound *N,N′*-dimethyl-2,3-di-*O*-methyl-L-tartaramide (Figure 1), abbreviated DMLT, using quantum mechanical calculations and also to investigate the effect of polarizable media. This is the subject of the present study.

In this work, the results of the gas-phase calculations for DMLT are reported first. Second, the effect of water, chloroform, and carbon tetrachloride solvents on the stability of the different conformers are compared and discussed in relation to the *gauche* oxygen effect. Third, polarization effects on the molecular dipole moments are

† Permanent address: Departamento de Química da Faculdade de Filosofia, Ciências e Letras de Ribeirão Preto, Universidade de São Paulo, Avenida Bandeirantes no. 3900, 14049-901, Ribeirão Preto, SP, Brazil.

[⊗] Abstract published in *Advance ACS Abstracts,* August 15, 1997.

(1) Abraham, R. J.; Banks, H. D.; Eliel, E. L.; Hofer, O.; Kaloustin, M. K. *J. Am. Chem. Soc.* **1972**, *94*, 1913.
(2) Eliel, E. L.; Hofer, O. *J. Am. Chem. Soc.* **1973**, *95*, 8041.
(3) (a) Altona, C.; Sundaralingam, M. *J. Am. Chem. Soc.* **1972**, *94*, 8205; (b) **1973**, *95*, 2333.
(4) Plavec, J.; Tong, W.; Chattopadhyaya, J. *J. Am. Chem. Soc.* **1993**, *115*, 9734.
(5) Thibaudeau, C.; Plavec, J.; Chattopadhyaya, J. *J. Am. Chem. Soc.* **1994**, *116*, 8033.
(6) (a) Olson, W. K.; Sussman, J. L. *J. Am. Chem. Soc.* **1982**, *104*, 270. (b) Olson, W. *J. Am. Chem. Soc.* **1982**, *104*, 278.
(7) Hossain, N.; Papchikhin, A.; Garg, N.; Fedorov, I.; Chattopadhyaya, J. *Nucleotides* **1993**, *12*, 499.
(8) Müller-Plathe, F.; van Gunsteren, W. F. *Macromolecules* **1994**, *27*, 6040.
(9) Sosanuma, K. *Macromolecules* **1995**, *28*, 8629.
(10) Gejji, S. P.; Tegenfeldt, J.; Lindgren, J. *Chem.Phys. Lett.* **1994**, *226*, 427.
(11) Alemán, C.; Martínez de Ilarduya, A; Giralt, E.; Muñoz-Guerra, S. *Tetrahedrom* **1996**, *52*, 8275.
(12) Yoshida, H.; Kaneko, I.; Matsura, H.; Ogawa, Y.; Tasumi, M. *Chem. Phys. Lett.* **1992**, *196*, 601.
(13) Tasaki, K.; Abe, A. *Polym. J.* **1985**, *17*, 641.
(14) Matsura, H.; Fukuhara, K.; Tamaoki, H. *J. Mol. Struct.* **1987**, *156*, 293.
(15) Inomata, K.; Abe, A. *J. Phys. Chem.* **1992**, *96*, 7934.
(16) Rodríguez-Galán, A.; Bou, J.; Muñoz-Guerra, S. *J. Polym. Sci., Polym. Chem. Ed.* **1992**, *30* , 713.
(17) Bou, J. J.; Iribarren, I.; Muñoz-Guerra, S. *Macromolecules* **1994**, *27*, 5263.
(18) Bou, J. J.; Muñoz-Guerra, S. *Polymer* **1995**, *36*, 181.
(19) Iribarren, I.; Alemán, C.; Bou, J. J.; Muñoz-Guerra, S. *Macromolecules* **1996**, *29*, 4397.
(20) Iribarren, I.; Alemán, C.; Regaño, C.; Bou, J.; Muñoz-Guerra, S. *Macromolecules* **1996**, *29*, 8413.

S0022-3263(96)02081-6 CCC: $14.00

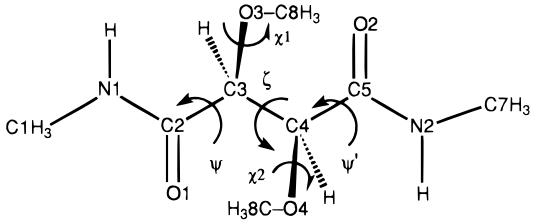

Figure 1. Scheme of the *N,N′*-dimethyl-2,3-di-*O*-methyl-L-tartaramide. Dihedral angles are defined according to the following atoms: $\Psi = \angle$N1−C2−C3−C4; $\xi = \angle$C2−C3−C4−C5; $\Psi' = \angle$C3−C4−C5−N2; $\chi_1 = \angle$C2−C3−O3−C7; $\chi_2 = \angle$C3−C4−O4−C8.

analyzed. Finally, the conformational characteristics of DMLT and PnDMLT are compared.

Methods

Gas-Phase Calculations. The DMLT is schematicaly shown in Figure 1, where the dihedral angle and atom notations used in this work are indicated. Since each of the five flexible dihedral angles Ψ, ζ, Ψ', χ_1 and χ_2 are expected to have three minima, 243 minima may be anticipated for the potential energy surface $E = E(\Psi, \zeta, \Psi', \chi_1, \chi_2)$. Thus, a complete exploration of the conformational space for DMLT using ab initio quantum mechanical methods is unaffordable from a computational point of view. Therefore, a reduced set of representative conformations, which includes the conformation previously found for the tartaric unit of PnDMLTs,[19,20] was selected in order to perform a rigorous ab initio study. Such structures were fully optimized with respect to all degrees of freedom at the HF/3-21G[21] level. However, previous studies suggested that the HF/3-21G level gives a poor description of the minima and reoptimization at higher levels of theory is required.[22−25] Therefore, all the minima found at the HF/3-21G level were subsequently reoptimized at the HF/6-31G(d)[26] level. Møller−Plesset perturbation treatment[27] at the MP2/6-31G(d) level was used to compute the electron correlation energy of the most important conformations. The nature of the different intramolecular interactions found in the low-energy conformations of DMLT has been analyzed at the semiempirical AM1[28] level using the energy partition scheme implemented in the MOPAC computer program.[29] These interactions have been compared with those found in small model dipeptides of amino acids.

Solvent-Phase Calculations. The free energies of solvation (ΔG_{sol}) were determined using a semiempirical AM1 adapted version[31−34] of the SCRF developed by Miertus, Scrocco, and Tomasi[35,36] (MST/AM1). According to this method, the ΔG_{sol} was determined as the addition of electrostatic and steric contributions (eq 1). The steric component was computed as the sum of the cavitation and van der Waals terms. The cavitation term was determined using Pierotti's scaled particle theory,[37] while the van der Waals term (eq 2) was evaluated by means of a linear relation with the molecular surface area[30−34]

$$\Delta G_{sol} = \Delta G_{ele} + \Delta G_{cav} + \Delta G_{vdW} \quad (1)$$

$$\Delta G_{vdW} = \sum_i \xi_i S_i \quad (2)$$

where S_i is the portion of the molecular surface area belonging to atom i and ξ_i is the hardness of atom i. Parameters defining the hardness of the different atom types in water,[32] chloroform,[38] and carbon tetrachloride[39] solvents were determined in previous parametrizations.

The electrostatic interaction between the solute and the solvent was computed using the MST-SCRF approach, in which the solvent is represented as a continuous dielectric, which reacts against the solute charge distribution generating a reaction field (V_R). The effect of the solvent reaction field on the solute is introduced as a perturbation operator in the solute Hamiltonian (eq 3). The perturbation operator is computed in terms of a set of point charges located at the solute/solvent interface *i.e.*, the solute cavity (eq 4).

$$(H^0 + V_R)\Psi = E\Psi \quad (3)$$

$$V_R = \sum_i q_i / |r_0 - r| \quad (4)$$

Such imaginary charges were determined by solving the Laplace equation at the solute/solvent interface. In all cases the solute/solvent interface was determined using a molecular shape algorithm.[30−34] Since the change of the molecular geometry upon solvation has a negligible effect on the thermodynamic parameters, only gas-phase-optimized geometries were used.[40] Previous studies indicated that the root mean square deviations between the experimental values of ΔG_{sol} and the values estimated at the MST/AM1 level are 1.0, 0.40 and 0.45 kcal/mol for water,[33] chloroform,[38] and carbon tetrachloride[39] solvents, respectively.

Ab initio calculations were performed with the Gaussian 94[41] computer program. Semiempirical calculations were performed with an adapted version of MOPAC93 revision 2,[29] which permits MST calculations with water, chloroform, and carbon tetrachloride solvents. All the calculations were run on an IBM-SP2 at the Centre de Supercomputació de Catalunya (CESCA).

Results and Discussion

Selection of the Starting Conformations in Geometry Optimizations. Since each geometry optimization at the HF/3-21G and HF/6-31G(d) levels takes more than 18 and 55 h of supercomputer CPU time (IBM-SP2), a reduced set of conformations was considered in this study. Considering the three backbone angles Ψ, ξ, and

(21) Binkley, J. S.; Pople, J. A.; Hehre, W. J. *J. Am. Chem. Soc.* **1980**, *102*, 939.
(22) Frey, R. F.; Coffin, J.; Newton, S. Q.; Ramek, M.; Cheng, V. K. W.; Momany, F. A.; Schäfer, L. *J. Am. Chem. Soc.* **1991**, *113*, 7129.
(23) Alemán, C.; Julia, L. *J. Phys. Chem.* **1996**, *100*, 1524.
(24) Navas, J. J.; Alemán, C.; Muñoz-Guerra, S. *J. Org. Chem.* **1996**, *61*, 6849.
(25) León, S.; Alemán, C.; García-Alvarez, M.; Muñoz-Guerra, S. *Struct. Chem.* **1997**, *8*, 39.
(26) Hariharan, P. C.; Pople, J. A. *Theoret. Chim. Acta* **1973**, *23*, 213.
(27) Møller, C.; Plesset, M. S. *Phys. Rev.* **1934**, *46*, 618.
(28) Dewar, M. J. S; Zoebisch, E. G.; Healy, E. H.; Stewart, J. J. P. *J. Am. Chem. Soc.* **1985**, *107*, 3902.
(29) Stewart, J. J. P. MOPAC 93 Revision 2; Fujitsu Limited, 1993. Adapted to perform MST calculations by F. J. Luque and M. Orozco.
(30) Bachs, M.; Luque, F. J.; Orozco, M. *J. Comput. Chem.* **1994**, *15*, 446.
(31) Orozco, M.; Luque, F. J. *Chem. Phys.* **1994**, *182*, 237.
(32) Orozco, M.; Bachs, M; Luque, F. J. *J. Comput. Chem.* **1995**, *16*, 563s.
(33) Luque, F. J.; Bachs, M.; Orozco, M. *J. Comput. Chem.* **1994**, *15*, 847.
(34) Luque, F. J.; Negre, M. J.; Orozco, M. *J. Phys. Chem.* **1993**, *97*, 4386.
(35) Miertus, S.; Scrocco, E.; Tomasi, J. *Chem. Phys.* **1981**, *65*, 239.
(36) Miertus, S.; Tomasi, J. *Chem. Phys.* **1982**, *65*, 239.
(37) Pierotti, R. A. *Chem. Rev.* **1976**, *76*, 717.
(38) Luque, F. J.; Zhang, Y.; Alemán, C.; Bachs, M.; Gao, J.; Orozco, M. *J. Phys. Chem.* **1996**, *100*, 4269.
(39) Luque, F. J.; Bachs, M.; Alemán, C.; Orozco, M. *J. Comput. Chem.* **1996**, *7*, 806.
(40) (a) Orozco, M.; Luque, F. J. *J. Am. Chem. Soc.* **1995**, *117*, 1378. (b) Alemán, C.; Navarro, E.; Puiggalí, J. *J. Org. Chem.* **1995**, *60*, 6135.
(41) Gaussian 94, Revision B.3., Frisch, M. J.; Trucks, H. B.; Schlegel, H. B.; Gill, P. M. W.; Johnson, B. G.; Robb, M. A.; Cheeseman, J. R.; Keith, T.; Petersson, G. A.; Montgomery, J. A.; Raghavachari, K.; Al-Laham, M. A.; Zakrzewski, V. G.; Ortiz, V. G.; Foresman, J. B.; Peng, C. Y.; Ayala, P. Y.; Chen, W.; Wong, M. W.; Andres, J. L.; Replogle, E. S.; Gomperts, R.; Martin, R. L.; Fox, D. J.; Binkley, J. S.; Defrees, D. J.; Baker, J.; Stewart, J. J. P.; Head-Gordon, M.; Gonzalez, C.; Pople, J. A. Gaussian, Inc., Pittsburgh PA, 1995.

Table 1. Conformational Angles (in degrees) and Relative Energies (in kcal/mol) for the Low-Energy Structures Computed at the HF/3-21G Level of DMLT

no.	Ψ	ξ	Ψ′	χ_1	χ_2	ΔE
I	46.4	45.5	46.4	73.0	-164.0	0.0
II	−143.8	−151.7	−143.8	178.2	−58.2	1.0
III	−125.4	169.3	−125.4	125.5	−114.6	1.0
IV	−133.2	−97.9	59.5	156.1	−167.8	4.1
V	−88.1	50.4	−160.0	70.2	60.2	6.8
VI	−148.8	60.4	−87.4	−173.2	−166.7	7.0
VII	−146.4	−70.8	133.9	152.1	−172.2	9.2
VIII	63.7	177.6	−15.9	−63.1	−160.1	11.9
IX	58.8	66.2	−86.2	174.8	−165.3	12.8

Table 2. Conformational Angles (in degrees) and Relative Energies (in kcal/mol) for the Low-Energy Structures Computed at the HF/6-31G(d) Level of DMLT

no.	Ψ	ξ	Ψ′	χ_1	χ_2	ΔE
I	53.4	46.7	53.4	77.1	−158.0	4.1
II	−144.0	−149.2	−144.0	164.9	−70.3	2.3
III	−123.5	179.0	−123.5	107.0	−131.0	0.0
IV	−129.2	−114.4	76.9	157.5	−167.8	6.3
V	−118.5	35.3	−159.0	89.0	60.6	7.2
VI	−123.6	48.0	−94.0	147.9	−158.9	5.9
VII	−147.8	−72.4	122.3	140.8	−172.9	5.8
VIII	59.7	−173.8	−19.7	−68.1	−152.5	10.1

Ψ′, 27 minima may be anticipated for the potential energy hypersurface $E = E(\Psi, \xi, \Psi')$ of the DMLT. A set of 14 of these structures was selected as starting geometries in HF/3-21G geometry optimizations. Side chain dihedral angles were initially considered in *trans* conformation. The starting conformations were

t t t	**t g$^+$ t**	**t g$^-$ t**
g$^+$ t g$^-$	**g$^+$ g$^+$ g$^-$**	**g$^+$ g$^-$ g$^-$**
g$^+$ g$^+$ t	**g$^+$ g$^+$ g$^+$**	**t t g$^+$**
t g$^+$ g$^-$	**t g$^-$ g$^+$**	**g$^+$ t g$^-$**
g$^+$ g$^-$ g$^+$	**g$^-$ g$^+$ t**	

where **g**$^+$, **g**$^-$, and **t** refer to *gauche*$^+$ (60°), *gauche*$^-$ (−60°), and *trans* (180°), respectively. Note that such structures contain a wide range of conformational patterns.

Gas-Phase Calculations. Geometry optimizations at the HF/3-21G level provided nine different low-energy conformations. Such structures were subsequently re-optimized at the HF/6-31G(d) level giving place to eight different low-energy structures. Thus, one of the structures found at the HF/3-21G level dissapeared upon geometry optimization at the HF/6-31G(d) level. Tables 1 and 2 display both the backbone and side chain dihedral angles for all the conformations found at the HF/3-21G and HF/6-31G(d) levels, respectively.

A comparative inspection of the results suggest that the agreement between HF/3-21G and HF/6-31G(d) optimized geometries is quite reasonable, the largest variations being in **V**. Thus, the results suggest that the HF/3-21G level is appropriate to perform an initial scanning of the potential energy hypersurface, but taking into account that it overestimates the number of stationary points. On the other hand, comparison between relative energies reveals a very poor agreement. The lowest energy structure at the HF/3-21G level is **I**, while both **II** and **III** are destabilized by 1.0 kcal/mol. Note, that at the HF/6-31G(d) level the lowest energy structure is **III**, whereas **I** and **II** are unfavored by 4.1 and 2.3 kcal/mol, respectively. Figure 2 displays the low-energy conformations **I**, **II**, and **III** computed at the HF/6-31G(d) level. The strong variation observed between the relative energies computed for **I** and **III** at the HF/3-21G and HF/6-31G(d) levels must be attributed to the fact that the latter method gives a much better representation of the *gauche* oxygen effect than the former one.[8−10] Thus, **III** is stabilized by a *gauche* effect in the O−C−C−O sequence, whereas **I** adopts a *trans* conformation for such a dihedral angle.

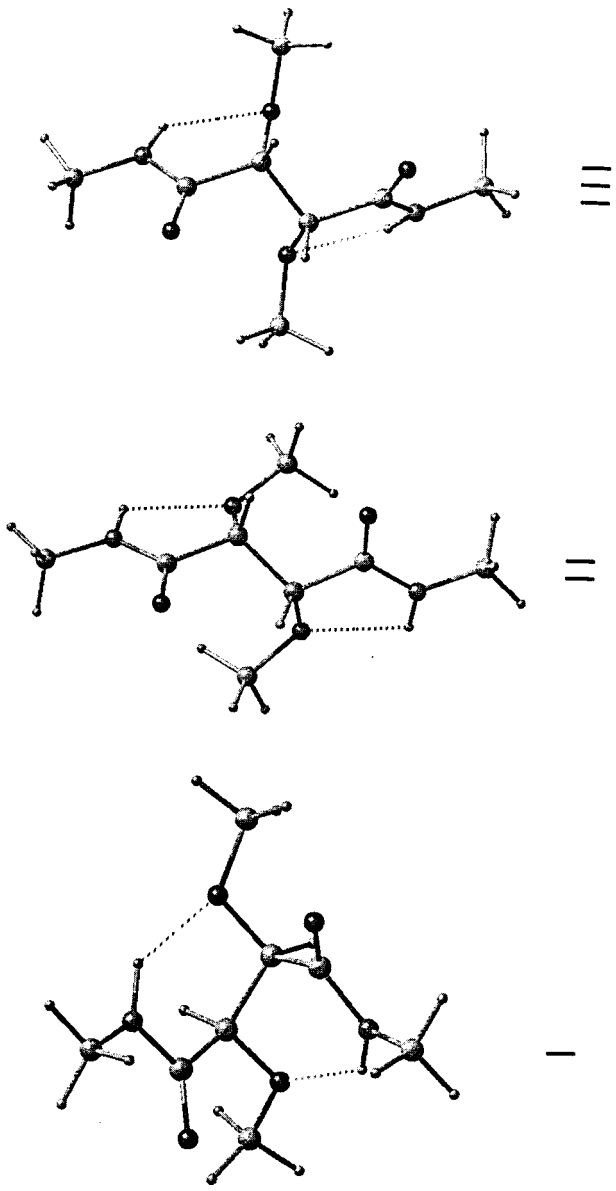

Figure 2. Low-energy conformations **I**, **II**, and **III** of *N*,*N*′-dimethyl-2,3-di-*O*-methyl-L-tartaramide computed at the HF/6-31G(d) level.

Figure 3a displays the low-energy conformation **VIII**, which is unfavored by 11.9 and 10.1 kcal/mol at the HF/3-21G and HF/6-31G(d) levels, respectively, with respect to the lowest energy one. This conformation is very similar to that found for the tartaric unit of PnDMLTs (Figure 3b), which was the lowest energy structure when the symmetry constraint $\Psi = -\Psi'$ was applied.[19] In such a crystal structure the carbonyls are arranged nearly in a *trans* conformation, determining the formation of intermolecular hydrogen bonds, whereas in **VIII** they deviate about 30° from such arrangement. The present results clearly point out that the crystal field can change the gas-phase relative energy order, as was recently suggested by Voight-Martin and co-workers.[42]

The most stricking feature of DMLT low-energy conformations is that in almost all the cases the hydrogen

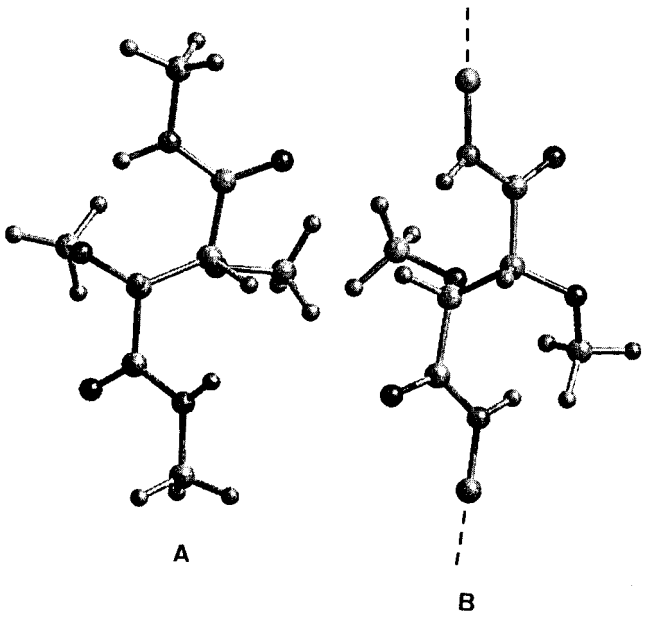

Figure 3. (a) Low-energy conformation **VIII** of *N,N′*-dimethyl-2,3-di-*O*-methyl-L-tartaramide computed at the HF/6-31G(d) level. (b) Conformation adopted by the tartaric acid moiety in PnDMLTs.

Table 3. Hydrogen-Bonding Geometries (distances in Å and angles in degrees) for the Low-Energy Conformations of DMLT Obtained at the HF/6-31G(d). Labels for the Donor and Acceptor Atoms Are Displayed in Figure 1

no.	atoms	type	*d*(H···O)	∠N−H···O
I	N1−H···O4	C_6	2.119	132.5
	N2−H···O3	C_6	2.118	132.5
II	N1−H1···O3	C_5	2.134	106.3
	N2−H···O4	C_5	2.137	106.3
III	N1−H···O3	C_5	2.184	107.1
	N2−H···O4	C_5	2.185	107.1
IV	N1−H···O3	C_5	2.125	106.9
	N2−H···O1	C_7	2.395	141.9
V	N1−H···O3	C_5	2.245	103.8
	N2−H···O4	C_5	2.281	104.3
VI	N1−H···O3	C_5	2.115	107.0
	N2−H···O1	C_7	2.477	122.2
VII	N1−H···O3	C_5	2.161	106.5
	N2−H···O4	C_5	2.648	101.9
VIII	N2−H···O4	C_5	2.033	135.6

atoms of the amide group form intramolecular interactions with the oxygen atoms of the side ether groups. Hydrogen bond parameters for all the HF/6-31G(d)-optimized geometries are displayed in Table 3. Note that two different kinds of amide···ether intramolecular interactions can be found. These are the C_5 (five-membered hydrogen bond system) and C_6 (six-membered hydrogen bond system), the former being more strained that the latter. An important feature is that **VIII** is able to form only one amide···ether interaction. Thus, the other amide group points in opposite direction to the side oxygen atom due to the *gauche*$^-$ conformation of the Ψ′ dihedral angle (see Figure 3a). Figure 3b shows the conformation found to the tartaric unit in PnDMLTs, which as was stated above has a backbone conformation similar to that of **VIII**. Note that no intramolecular interaction is present in the crystal structure of this family of polyamides since side chains adopt a *skew* conformation in order to improve the packing interactions. Thus, in **VIII** the χ_1 and χ_1' angles adopt *gauche*$^-$ and *trans* conformations, respectively, whereas in PnDMLTs they are $\chi_1 = -\chi_1' \approx 101°$.

Table 4. Energy Partitioning Using the AM1 Method (Energy Contributions Are in eV and Hydrogen-Bonding Distances in Å). J, C, and E Refer to the Resonance, Coulombic, and Total Energies, Respectively

no.	atoms	type	*d*(H···O)	J	C	E
I	N1−H···O4	C_6	2.119	−0.163	−0.424	−0.611
	N2−H···O3	C_6	2.118	−0.164	−0.428	−0.611
III	N1−H···O3	C_5	2.184	−0.123	−0.393	−0.530
	N2−H···O4	C_5	2.185	−0.123	−0.393	−0.531
IV	N1−H···O3	C_5	2.125	−0.146	−0.421	−0.582
	N2−H···O1	C_7	2.395	−0.062	−0.567	−0.637

Another type of intramolecular interactions was detected in some of the low-energy conformations of DMLT. Conformers **IV** and **VI** form a C_7 (seven-membered hydrogen bond system) between the two amide groups of the main chain. As it can be seen in Table 3, these conformers also have a C_5 amide···ether interaction, this being much more strained than the amide···amide interaction. Apparently, the amide···amide interactions found in DMLT seem to be weaker than those observed in dipeptides of usual amino acids. Thus, it is well-known that structures with a C_7 amide···amide interaction are the lowest energy conformations in model dipeptides of glycine and alanine.[43,44] Furthermore, such interactions give place to the 2_7-ribbon structure, which is strongly favored in peptides with a small number of amino acids.[45,46] However, for DMLT conformers with C_7 amide···amide interactions are destabilized by at least 5.9 kcal/mol.

In order to compare both the strengths of amide···amide and amide···ether interactions in DMLT and the differences between the amide···amide interactions in DMLT and dipeptides of amino acids, we have used the energy partition scheme implemented in MOPAC (ENPART). This provides a qualitative estimation of the intensity of intramolecular bonds as was indicated in our previous works.[47,48] With this partition scheme it is possible to understand the origin of the interactions taking into account two terms, the electrostatic contribution and the overlap of the molecular orbitals, the latter being indicated by the resonance energy. To our knowledge, there is no other partition scheme that may be used in intramolecular interactions, in opposition to intermolecular interactions.

In order to make a comparison with amide···amide interactions in peptides, the C_7 conformation of α,α-aminoisobutyric acid dipeptide, *i.e.*, 2-acetyl-2-*N*-dimethylpropanamide, was optimized at the HF/6-31G(d) level. The ENPART calculations indicate that the strengths of the C_7 amide···amide interactions in α,α-aminoisobutyric acid dipeptide and DMLT are similar. On the other hand, Table 4 shows the energy contributions for the

(42) Voight-Martin, I. G.; Simon, P.; Yan, D.; Yakimansky, A.; Bauer, S.; Ringsdorf, H. *Macromolecules* **1995**, *28*, 243.

(43) Alemán, C.; Pérez, J. J. *J. Comput. Aided Mol. Design* **1993**, *7*, 241.

(44) Shang, H. S.; Head-Gordon, T. *J. Am. Chem. Soc.* **1994**, *116*, 1528.

(45) Casanovas, J.; Alemán, C. *J. Comput. Aided Mol. Design* **1994**, *8*, 441.

(46) Vega, M. C.; Alemán, C; Giralt, E.; Pérez, J. J. *J. Biomol. Struct. Dyn.* **1992**, *10*, 1.

(47) Pereira, G. K.; Donate, P. M.; Galembeck, S. E. *J. Mol. Struct. (Theochem)* **1996**, *363*, 87.

(48) Pereira, G. K.; Donate, P. M.; Galembeck, S. E. *J. Mol. Struct. (Theochem)*, in press.

(49) Alemán, C.; Casanovas, J. *J. Chem. Soc., Perkin Trans. 2* **1994**, 563.

Table 5. O−C−C−O and O═C−C−O Dihedral Angles (in degrees) for the Low-Energy Structures Computed at the HF/6-31G(d) Level of DMLT

no.	O1═C−C−O3	O3−C−C−O4	O2═C−C−O4	pattern[a]
I	−30.2	159.5	−30.2	**g t g**
II	164.9	−35.8	164.9	**t g t**
III	179.3	−67.8	179.3	**t g t**
IV	177.1	0.0	18.5	**t c c**
V	−172.3	45.9	159.5	**t g t**
VI	−179.0	158.8	−151.1	**t t t**
VII	157.2	47.3	55.2	**t g g**
VIII	9.7	−68.1	−76.0	**c g g**

[a] **t**, **g**, and **c** refer to *trans*, *gauche*, and *cis*, respectively.

amide···amide and amide···ether interactions in DMLT. Note that the former is more intense than the later. This is in good agreement with our previous results on the strength of the hydrogen bond between the amide group and the alkoxy oxygen atom of a ester group.[50] Another interesting feature is the different nature of these two intramolecular interactions. Thus, the amide···amide is mainly an electrostatic interaction, where the amide···ether has also a component that may be attributed to the overlap of orbitals. Regarding the amide···ether interactions, the gain of energy produced by the C_5 interaction is lower than that of the C_6 indicating that the latter is stronger than the former (see Table 4).

Table 5 displays the O═C−C−C−O and O−C−C−O dihedral angles measured for the HF/6-31G(d) low-energy conformations. Note that four different situations can be defined according to the computed values. For **II**, **III**, and **V** the two O═C−C−O sequences are arranged *trans*, whereas the O−C−C−O dihedral angle adopts a *gauche* conformation. The reversed situation appears in **I**, where the O═C−C−O and O−C−C−O dihedral angles adopt *gauche* and *trans* conformations respectively. For **IV** and **VI** the three dihedral angles adopt *trans* and/or *cis* conformations losing the *gauche* oxygen effect in the O−C−C−O sequence. Finally, in **VII** and **VIII** one of the two O═C−C−O angles adopts a *gauche* conformation similar to the O−C−C−O one, whereas the other is arranged *trans* and *cis*, respectively. Conformers **I**, **VII**, and **VIII**, which have at least an O═C−C−O sequence *gauche*, are 4.1, 5.8, and 10.1 kcal/mol destabilized with respect to the lowest energy one. This feature suggests that no extra stabilization is obtained when the O═C−C−O dihedral angles are arranged *gauche*.

In order to study the effect of the electronic correlation on the *gauche* oxygen effect, we computed the energies of **I**, **III**, **VI**, and **VII** at the MP2/6-31G(d) level using the HF/6-31G(d) molecular geometries. Note that such conformers present important differences in O−C−C−O and O═C−C−O dihedral angles (see Table 5). The MP2 results were very similar to those obtained at the HF level from a qualitative point of view. However, the MP2 relative energies are lower than the HF ones. Thus, **I**, **VI**, and **VII** were 1.5, 4.4, and 3.7 kcal/mol less favored than **III**, respectively. The energy between **I** and the lowest energy conformation **III** is reduced by 2.6 kcal/mol when the level of theory changes from MP2 to HF. However, what seems to be clear from the present results is that the *gauche* conformation is favored for the O−C−C−O sequence, whereas no *gauche* oxygen effect was detected for the O═C−C−O one.

(50) Alemán, C.; Navas, J. J.; Muñoz-Guerra, S. *J. Phys. Chem.* **1995**, *99*, 17653.

Table 6. Solvation (ΔG_{sol}) and Conformational (ΔG_{conf}) Free Energies (in kcal/mol) in Aqueous Solution for the Low-Energy Structures of DMLT. The ΔG_{sol} Is Descomposed into the Electrostatic and Steric [Cavitation + van der Waals] Terms

no.	ΔG_{ele}	ΔG_{ster}	ΔG_{sol}	$\Delta\Delta G_{sol}$	$\Delta\Delta G_{conf}$
I	−13.4	3.9	−9.5	2.7	5.8
II	−14.1	4.1	−10.0	2.2	3.5
III	−15.2	4.0	−11.2	1.0	0.0
IV	−14.2	4.2	−10.0	2.2	7.5
V	−13.9	3.9	−10.0	2.2	8.4
VI	−16.5	4.3	−12.2	0.0	4.9
VII	−14.9	4.0	−10.9	1.3	6.1
VIII	−15.7	3.9	−11.8	0.4	9.5

Table 7. Dipole Moments (in Debyes) for the Low-Energy Structures of DMLT Computed at the HF/6-31G(d) Level

no.	μ	no.	μ
I	2.91	**V**	1.75
II	4.46	**VI**	6.79
III	4.23	**VII**	3.58
IV	1.17	**VIII**	4.83

Solution Phase. Solvation free energies (ΔG_{sol}) for DMLT in aqueous, chloroform, and carbon tetrachloride solutions are listed in Tables 6, 7, and 8, respectively, where the electrostatic and steric [cavitation + van der Waals] contributions are included. The conformational free energy difference (ΔG_{conf}) in solution was estimated by adding $\Delta\Delta G_{sol}$ to the gas-phase relative energy (eq 5).

$$\Delta G_{conf} \approx \Delta E + \Delta\Delta G_{sol} \quad (5)$$

The results in Table 6, which shows the different free energy values in aqueous solution, reveal that the origin of the differences in ΔG_{sol} lies in the electrostatic term. Thus, the steric term ranges from 3.9 to 4.3 kcal/mol for the different conformers, whereas the electrostatic one varies from −13.4 to −16.5 kcal/mol. This trend can be explained from the dipole moments of the different conformers, which are listed in Table 7. In general terms, it should be noted that structures with large dipole moments have better electrostatic interactions with the solvent. Inspection of the $\Delta\Delta G_{conf}$ values indicates that in general terms water does not introduce drastic changes in the stability of the different conformers. However, interesting features can be extracted from a detailed comparison between the gas-phase and aqueous solution relative energies for **I**, **II**, and **III**. Thus, the change from the gas phase to aqueous solution increases the destabilization of **I** with respect to **III** by 1.4 kcal/mol. This feature clearly points out that the O−C−C−O *gauche* oxygen effect is favored by the presence of a polarizable environment such as water in agreement with previous experimental studies on 1,2-DME.[12−15] Our results suggest that such stabilization is due to an increase of the electrostatic interactions with solvent. On the other hand, comparison between **II** and **III** indicates that in aqueous solution the former is less favored than in gas phase, indicating that no *gauche* oxygen effect appears in the sequence O═C−C−O.

Results for organic solvents are displayed in Table 8. Notice that ΔG_{sol} are slightly lower in chloroform solution than in water and carbon tetrachloride, indicating a slightly higher affinity of DMLT by the former than by the latters. An inspection to the ΔG_{sol} contributions indicates that in organic solvents the steric is the leading term. This must be attributed to the electronic structure of the solvents.[38,39]

Table 8. Solvation (ΔG_{sol}) and Conformational (ΔG_{conf}) Free Energies (in kcal/mol) in Chloroform and Carbon Tetrachloride (roman and italic, respectively) Solution for the Low-Energy Structures of DMLT. The ΔG_{sol} Is Descomposed into the Electrostatic and Steric [Cavitation + van der Waals] Terms

no.	ΔG_{ele}	ΔG_{ster}	ΔG_{sol}	$\Delta\Delta G_{sol}$	$\Delta\Delta G_{conf}$
I	−2.6	−9.2	−11.8	0.9	4.8
	−1.1	−8.6	*−9.7*	*0.6*	*4.5*
II	−2.9	−9.3	−12.2	0.5	2.6
	−1.2	*−8.7*	*−9.9*	*0.4*	*2.5*
III	−3.1	−9.4	−12.5	0.2	0.0
	−1.3	*−8.9*	*−10.2*	*0.2*	*0.0*
IV	−2.6	−9.2	−11.8	0.9	7.0
	−1.1	*−8.8*	*−9.9*	*0.4*	*6.5*
V	−2.7	−9.0	−11.7	1.0	8.0
	−1.1	*−8.5*	*−9.6*	*0.7*	*7.7*
VI	−3.6	−9.1	−12.7	0.0	5.7
	−1.5	*−8.8*	*−10.3*	*0.0*	*5.7*
VII	−3.0	−9.3	−12.3	0.4	6.0
	−1.2	*−8.6*	*−9.8*	*0.5*	*6.1*
VIII	−3.5	−9.2	−12.7	0.0	9.9
	−1.5	*−8.6*	*−10.1*	*0.2*	*10.1*

Organic solvents have very small effects on the stability of the different conformers. Thus, the highest values of $\Delta\Delta G_{sol}$ are 1.0 and 0.7 kcal/mol in chloroform and carbon tetrachloride solutions, respectively. However, inspection to the results obtained for **I** and **III** reveals that organic solvents have a small influence on the *gauche* oxygen effect. Thus, conformer **I** is unfavored with respect to **III** by 4.8 and 4.5 kcal/mol in chloroform and carbon tetrachloride, respectively. These values are larger than that obtained in the gas phase but smaller than the relative energy predicted in aqueous solution. The amount of stabilization of the *gauche* oxygen effect in **III** due to the polarizable environment is 1.7, 0.7, and 0.4 kcal/mol in water, chloroform, and carbon tetrachloride, respectively. The present results confirm not only that polarizable environments stabilize the *gauche* oxygen effect but also that the amount of stabilization depends on the electronic characteristics of the solvent.

Conclusions

In this work we are concerned with several structural properties observed in the low-energy conformers of DMLT. The results in the gas phase clearly indicate that the lowest energy structure is stabilized by the *gauche* oxygen effect in the O−C−C−O sequence, whereas such an effect does not exist in the two O=C−C−O sequences. On the other hand, a low-energy structure similar to that observed in the solid state was investigated. Results indicate that such conformation is 10.1 kcal/mol unfavored with respect to the lowest energy one, suggesting that in the solid state it is mainly stabilized by packing interactions. We have tried to account for polarizable environment effects by MST calculations with three different solvents: water, chloroform, and carbon tetrachloride. The results indicate that the *gauche* oxygen effect is more favored in solution than in the gas phase. Furthermore, the amount of stabilization depends on the electronic nature of the solvent. For instance, the *gauche* oxygen effect is much more favored in aqueous solution than in organic solvents.

Acknowledgment. We are indebted to CESCA for computational facilities and to Dr. M. Orozco and Dr. F. J. Luque for making available to us their version of MOPAC93 adapted to perform MST calculations. Authors are indebted to Prof. S. Muñoz-Guerra for helpful suggestions. This work was supported by grant from the CICYT (MAT-96-1181-CO3). S.E.G. thanks to Brazilian fundation FAPESP for the financial support when in Spain.

JO962081G